Chinese Herbal Medicines 17 (2025) 156–165

Contents lists available at ScienceDirect

Chinese Herbal Medicines

journal homepage: www.elsevier.com/locate/chmed

Original Article

Intratumoral injection of two dosage forms of paclitaxel nanoparticles combined with photothermal therapy for breast cancer

Lina Sun [a], Cuiling Zuo [a], Baonan Ma [a], Xinxin Liu [b], Yifei Guo [a], Xiangtao Wang [a,*], Meihua Han [a,*]

[a] Institute of Medicinal Plant Development, Chinese Academy of Medical Sciences & Peking Union Medical College, Beijing 100193, China
[b] Research Center of Pharmaceutical Engineering Technology, Harbin University of Commerce, Heilongjiang 150076, China

ARTICLE INFO

Article history:
Received 25 October 2023
Revised 20 May 2024
Accepted 18 June 2024
Available online 20 June 2024

Keywords:
breast cancer
combination therapy
paclitaxel
photothermal therapy
polypyrrole

ABSTRACT

Objective: In order to enhance the efficacy of anti-breast cancer, paclitaxel nanoparticles (PTX NPs) and polypyrrole nanoparticles (PPy NPs) were combined with photothermal therapy and chemotherapy. At the same time, the two dosage forms of PTX NPs and PTX NPs gel were compared.
Methods: PTX NPs were prepared by self-assembly method, and then the cytotoxicity *in vitro* was investigated by Methyl thiazolyl tetrazolium (MTT) and other methods, and the efficacy and side effects *in vivo* were further investigated.
Results: The average hydrated diameter, PDI and electric potential of PTX NPs were (210.20 ± 1.57) nm, (0.081 ± 0.003) mV and (15.80 ± 0.35) mV, respectively. MTT results showed that the IC_{50} value of PTX NPs on 4 T1 cells was 0.490 μg/mL, while that of PTX injection was 1.737 μg/mL. The cell inhibitory effect of PTX NPs was about 3.5 times higher than that of PTX injection. The tumor inhibition rates of PTX NPs and gel were 48.64% and 56.79%, respectively. Together with local photothermal stimulation, the tumor inhibition rate of the PTX NPs reached 91.05%, surpassing that of the gel under the same conditions (48.98%), moreover, the organ index and H&E staining results of PTX NPs showed a decrease in toxicity.
Conclusion: This combination therapy can significantly enhance the effect of anti-breast cancer, and the synergistic effect of chemotherapy and light and heat provides a feasible and effective strategy for the treatment of tumor.

1. Introduction

Cancer is one of the leading causes of death in the world, and the number of cancer deaths is expected to continue to increase. Breast cancer is one of the most prevalent cancers in the world, accounting for approximately 25% of all malignancies (Ghoncheh, Pournamdar, & Salehiniya, 2016). Although the majority of breast cancer cases are treatable, the 5-year survival rate for patients with metastatic breast cancer is 22%, with distant organs metastases being the leading cause of deaths (Chen et al., 2017; Wu et al., 2017; Qi et al., 2022). At present, among the common clinical treatments, including radiotherapy and chemotherapy, hormone therapy, ligands, monoclonal antibodies, targeted nano-drugs and individualized therapy, chemotherapy is the most commonly used and effective method. To reduce breast cancer mortality and alleviate the burden on healthcare systems, global efforts are needed to improve cancer prevention and treatment strategies (Arnold et al., 2022; Fahad Ullah, 2019; Katsura, Ogunmwonyi, Kankam, & Saha, 2022).

Paclitaxel (PTX) is a natural anticancer drug extracted from Taxus, which has significant therapeutic effect on a variety of solid tumors (Han et al., 2016; Weaver, 2014; Yu, Lou, Ma, & Najafi, 2022; L. Zhu & Chen, 2019). However, its water solubility is very low, and it is associated with serious side effects such as nerve and renal toxicity, as well as allergic reactions (Choudhury et al., 2017; Singla, Garg, & Aggarwal, 2002).

Local tumor chemotherapy is a treatment method where drugs or preparations are directly injected or perfused into the tumor, aiming to ingest by the tumor or tumor cells and effectively inhibit tumor growth (Melero, Castanon, Alvarez, Champiat, & Marabelle, 2021; S. Zhu, Dou, & Huang, 2018). Due to the high drug concentration in the lesion site and less drug distribution in the surrounding healthy tissue, local chemotherapy minimizes systemic exposure and extra-target toxicity. Although this method can reduce the side effects of drugs, it can increases the risk of second cancer incidence (Kievit & Zhang, 2011; Nolsoe et al., 1993; Vogel & Venugopalan, 2003). In order to improve the recovery effect of patients, the combination therapy with photothermal therapy was taken.

* Corresponding authors.
E-mail addresses: xtaowang@163.com (X. Wang), hanmeihua727@163.com (M. Han).

https://doi.org/10.1016/j.chmed.2024.06.001
1674-6384/

Photothermal therapy is a non-invasive method for cancer treatment, which uses near-infrared (NIR) or other heat sources to raise the temperature of a specific area to treat cancer (Chu & Dupuy, 2014; Huang, El-Sayed, Qian, & El-Sayed, 2006; Lal, Clare, & Halas, 2008). Polypyrrole (PPy) based nanomaterials are often used as photothermal materials due to their convenient synthesis methods and good biocompatibility (Chen, Fang, Tang, & Zheng, 2012; Ibrahim, Hanafi, El-Tayeb, & Sliem, 2022; Li et al., 2019; Tian, Zhang, Tang, Zhou, & Yang, 2016; Yang et al., 2012; Zha, Yue, Ren, & Dai, 2013). In addition, PPy has strong absorption performance at 808 nm, and its photothermal conversion efficiency can be up to 44.7 %, which can effectively kill tumor cancer cells (Chen et al., 2012). The photothermal conversion characteristics of PPy make the nanogel have dual response to temperature and near-infrared light (Theune et al., 2019).

Thermosensitive gel is a innovative type of intelligent sustained-release preparation, which can gelatinize rapidly to form a semisolid reservoir at the drug administration site under physiological conditions (Kim, Shin, Kim, Lee, & Lee, 2022). By utilizing the PTX drug-loading gel system, it can slow down the release of drug, and prevent sudden release, and then reduce the systemic side effects of drugs, and enhance the locally effective concentration of drug (Ahmed, Alhareth, & Mignet, 2020; Chen et al., 2021; Korzhikov-Vlakh & Tennikova, 2021). The gelation process of thermosensitive gel does not require additional additives or chemical reactions, and it takes advantage of the organism's own temperature as a physical trigger. Consequently, since its discovery, it has become a prominent research focus in the medical field. Thermosensitive gel has been successfully applied to various drug delivery routes, including mucosal drug delivery, injection drug delivery, rectal drug delivery, and transdermal drug delivery (Choi, Kwon, Choi, Hahn, & Kim, 2021; Ding et al., 2018).

In this study, photothermal combined with local injection of PTX NPs and gel were conducted to further explore the treatment of breast cancer, hoping to provide new ideas for the clinical treatment of tumors.

2. Materials and methods

2.1. Materials

PTX (Beijing Coincidence Co., Ltd., China, Batch No. Cp202-160802, quality score > 99.0%); PCL_{2000}-$mPEG_{2000}$ (Jinan Dai gang Biological Engineering Co., Ltd., China); Poloxamer 407 (Wuhan New Earth Environmental Protection Material Co., China); Poloxamer 188 (Sigma, USA); Polyvinyl alcohol (China National Pharmaceutical Group Chemical Reagent Co., Ltd., Shanghai, China). Ferric chloride hexahydrate and pyrrole (Beijing Bailingway Technology Co., Ltd., China); RPMI 1640, phosphate buffer (PBS), fetal bovine serum and penicillin (Beijing Qinghege Co., Ltd., China); 96-well sterile culture plates (Corning Co., Ltd., USA); The other reagents were analytically pure. KM-200DE Chinese liquid crystal ultrasonic cleaner (Kunshan Meimei Ultrasonic Instrument Co., Ltd., China); Hitech Laboratory ultrapure Water Machine (Shanghai Hetai Instrument Co., Ltd., China); Zetasizer Nano ZS Granulometer (Malvern Instruments, UK); 808 nm infrared semiconductor laser (model: MW-GX-808) (Changchun Laishi Optoelectronics Co., Ltd., China) (Zuo et al., 2022).

2.2. Cell lines and animals

4 T1 cells (The Cell Resource Center of the Institute of Basic Medical Sciences, Chinese Academy of Medical Sciences). Cells at 37 °C and 5% CO_2 (Sanyo, Osaka, Japan) were cultured in RPMI-1640 medium (Hy Clone, Logan City, UT, USA) containing 10% FBS, 100 U/mL penicillin and streptomycin (Gibco, St Louis, MO, USA). Female Balb/c mice, 6–8 weeks old, weighing (20 ± 2) g (Beijing Weitong Lihua Laboratory Animal Company). The animals were accustomed to 25 °C standard feed for one week (Zuo et al., 2022). The experimental protocols were approved by the Chinese Institute of Medicinal Plants (Beijing, China). Affidavit of Approval of Animal Ethical and Welfare Approval Number: SLXD-20220303029.

2.3. Preparation of PTX-PPy nanohydrogel

2.3.1. Preparation of PTX NPs

Ten mg PTX and 10 mg PCL_{2000}-$mPEG_{2000}$ carriers were dissolved in 1 mL acetone and injected into 10 mL deionized water by ultrasound. The organic solvent acetone was removed by spinning 5 min at 40 °C and homogenized for 10 times under high pressure (Kim & Lee, 2001).

2.3.2. Preparation of PPy NPs

Polyvinyl alcohol (98.88 mg, 12 mg/mL) was added to 8.24 mL deionized water, then $FeCl_3{\cdot}6H_2O$ (514.80 mg) was added, heated to 95 °C, mixed and stirred for 1 h. Then the mixed solution was transferred to an ice water bath, and 57.20 μL of pyrrole monomer solution was added. The mixture was stirred in the ice bath for 4 h, centrifuged at 13 000 r/min for 10 min, dispersed in deionized water and washed with water for 3 times, and then ultrasonically washed with acetone for 3 times. The precipitate was dispersed in water, and finally filtered with 0.45 μm micropore filter membrane (Li et al., 2019; Yang et al., 2012).

2.3.3. Preparation of blank hydrogels

Add 100 mL of physiological saline into the beaker, then sprinkle 2.05 g of Poloxamer 407 and 0.20 g of Poloxamer 188 evenly on the water surface, and then place them in a refrigerator at 4 °C for swelling for 12 h to obtain a clear and transparent blank gel solution (Zeng, Dumortier, Maury, Mignet, & Boudy, 2014).

2.3.4. Preparation of drug-loaded nanoparticle gels

Firstly, 10 mL of 1 mg/mL PTX NPs was added into a 50 mL small beaker, then 2.05 g Poloxamer 407, 0.20 g Poloxamer 188 and 5 mg PPy NPs dry solids were weighed into the beaker, mixed evenly, and placed in the refrigerator at 4 °C overnight.

2.4. Characterization of nanoparticles

2.4.1. Particle diameter and morphology

The size, polydispersion index (PDI) and zeta potential of PTX NPs and PPy NPs were determined by dynamic light scattering (DLS, Zeta Sizer Nano ZS, Malvern Instruments, UK) three times at room temperature. The surface morphology was observed by Transmission electron microscope (TEM) (JEOL Ltd.). The nanoparticles were diluted with water to clarify, and then dropped on copper mesh. After drying, the nanoparticles were stained with 2% (W/V) uranyl acetate. The morphology and size of the particles were observed by TEM.

2.4.2. Investigation of medium stability

PTX NPs and PPy NPs were mixed with an equal volume of 1.8% NaCl, 10% glucose and PBS, respectively, and incubated at 37 °C. The changes of particle size and PDI were measured at different time points, and each sample was measured three times.

2.5. Determination of phase transition temperature

The critical gelation temperature of blank gel was determined by stirring method. The 10 mL temperature-sensitive gel solution

have been determined in a Xillin flask, added to the agitator, and inserted into a probe-based thermometer (accuracy: 0.1 °C) over a magnetic agitator. The rotation speed was set to 150 r/min, and the temperature of the gel liquid was kept rising slowly to make the temperature rise rate of the gel liquid be 1–2 °C/min. The temperature when the gel was completely condensed (without flow) was observed and recorded, which was the phase transition temperature. Three samples were measured in parallel, and the average value was taken.

2.6. Investigation of photothermal conversion performance

1 mL of three PPy NPs with different concentrations (1, 0.5 and 0.25 mg/mL) was added into the EP tube, and the temperature sensor was inserted. After the indicator number was stable, the temperature was denoted as 0 s nanoparticles temperature, and the fixed power was 2.5 W/cm^2. The nanoparticles temperature was recorded every 30 s, and then the power was adjusted to 3 W/cm^2 and 3.5 W/cm^2, respectively. The above operation process was repeated to investigate the change of temperature rise (Zuo et al., 2022).

2.7. In vitro cell experiment

2.7.1. In vitro cytotoxicity assay

The cytotoxic effects of different drugs and treatments on 4 T1 cells *in vitro* were determined by Methyl thiazolyl tetrazolium (MTT) (Habibi, Sadat Shandiz, Salehzadeh, & Moradi-Shoeili, 2020; Sun et al., 2022). 4 T1 cells were simply inoculated on a 96-well plate and cultured for 24 h (8 000 cells/well, 5% CO_2, 37 °C). PPy NPs, PTX NPs and PTX injection were diluted with RPMI 1 640 medium. PPy NPs, PTX NPs and commercially available PTX solution were added at different concentrations of 200 μL, respectively (The concentrations of PPy NPs were 0.05, 0.1, 0.5, 1, 1.5, 2.5, 3, 5, 20, 40, 50 mg/mL; PTX NPs were 0.02, 0.04, 0.2, 10, 12, 15, 20 μg/mL; PTX injection were 0.01, 0.1, 1, 2, 5, 10, 50, 100 μg/mL). PPy NPs was divided into two groups, one of which was irradiated by NIR for 3 min after the addition of drug-containing medium. After 4 T1 cells were incubated for 48 h, 20 μL 5 mg/mL tetrazolium salt solution was added to each well, and then continued to incubate for 4 h, and finally 200 μL dimethyl sulfoxide was added to each well. Detection was performed at 570 nm using an ELISA plate reader (Biotek, USA). Cell inhibition rate was calculated by Eq. (1):

$$\textit{Cell inhibition rate}\ (\%) = 1 - (ODe/ODc) \times 100 \quad (1)$$

ODe and ODc were the average optical densities of the experimental group and control group. The half inhibitory concentration (IC_{50}) of the cells was calculated by GraphPad Prism software (GraphPad Software, Inc., La Jolla, CA, USA).

2.7.2. In vitro cell uptake experiment

4 T1 cells cultured in logarithmic growth phase were inoculated in 24-well plates (1×10^5/well) and cultured in 37 °C, 5% carbon dioxide for 24 h. Coumarin-6 labeled PTX NPs, PTX NPs Gel, PTX NPs + NIR and PTX NPs Gel + NIR were added respectively. The concentration of PTX was 20 μg/mL and PPy NPs was 0.5 mg/mL. After 1 h of culture, the drug culture medium was removed and washed with PBS. Add 4% paraformaldehyde to fix for 20 min and rinse with PBS. DAPI staining was performed for 10 min. The cells in the combined administration group were irradiated with near infrared radiation of wavelength 808 nm and power 3.5 W/cm^2 for 350 s. The uptake of PTX by cells was observed by laser confocal microscope.

2.8. Antitumor activity in vivo

2.8.1. Study on biological distribution in vivo

The adherent 4 T1 cells in logarithmic growth phase were adjusted to 6.0×10^6cells /mL with aseptic PBS. 4 T1 cells 0.2 mL was subcutaneously inoculated into the axilla of female Balb/c mice. When the tumor grew to a certain volume, 15 Balb/c 4 T1 tumor-bearing mice were selected and randomly divided into five groups. PTX injection group (8 mg/kg), PTX NPs group, PTX NPs Gel group, PTX NPs + NIR group and PTX NPs Gel + NIR group were injected intravenously with Dir labeled drugs, respectively. The dose of PTX in each group of intratumoral injection was 2 mg/kg. Each group was treated with PPy NPs of 2.5 mg/kg and 808 nm of 3.5 W/cm^2 respectively. The dynamic drug distribution was observed at 1, 4, 6, 8, 12 and 24 h after intratumoral administration. After 24 h of unified administration, the mice were euthanized. The heart, liver, spleen, lung, kidney and tumor were dissected for *in vivo* imaging.

2.8.2. Establishment of animal models

Under sterile conditions, 4 T1 cells were cultured *in vitro* to the logarithmic growth stage. The adherent cells were digested into cell suspension with trypsin, and the concentration of cell suspension was adjusted to 6.0×10^6 cells/mL with sterile PBS. Eighty healthy and active female Balb/c mice weighing 20–22 g were inoculated with 0.2 mL of 4 T1 cell suspension in the left armpit of each mouse. When the tumor volume was relatively close to 150 mm^3, 48 mice with the same tumor volume were selected for the experiment (Zuo et al., 2022).

2.8.3. Experimental grouping and administration

The selected tumor-bearing mice were randomly divided into eight groups, with six mice in each group. All mice were given normal diet. Intravenous administration group was given once every two days for a total of 12 d, 7 times; In the intratumoral injection group, three doses were administered on the 0, 4, and 8 d, respectively. Grouping and administration were shown in Table 1.

2.8.4. Pharmacodynamic evaluation index

After the first dose, the mice were weighed every other day with an electronic scale to an accuracy of 0.1 g. The activity, sleep, hair color and death of mice were observed daily during the whole course of drug administration. The length (a) and width (b) of the mouse tumor were measured and recorded every other day with electronic vernier calipers, accurate to 0.01 mm. On the 12th day of treatment, the mice were euthanized and dissected. The tumor, liver and spleen were weighed. The tumor volume was calculated according to Eq. (2), and the tumor inhibition rate was calculated according to Eq. (3). Eq. (4) was used to calculate the indexes of liver and spleen of mice.

$$V = (a \times b_2)/2 \quad (2)$$

Table 1
Grouping and drug administration.

Groups	Mode of administration	Volume/mL
Saline	i.v	0.2
PTX Injection (8 mg/kg)	i.v	0.2
PPy NPs + NIR*	i.t	0.1
PPy NPs Gel + NIR*	i.t	0.1
PTX NPs (2 mg/kg)	i.t	0.1
PTX NPs Gel (2 mg/kg)	i.t	0.1
PTX NPs (2 mg/kg) + NIR*	i.t	0.1
PTX NPs Gel (2 mg/kg) + NIR*	i.t	0.1

i.v: Tail-vein injection; i.t: Intratumoral injection; *Near-infrared processing parameters: 808 nm, 3.5 W/cm^2, 350 s.

$$TSR\ (\%) = W_t/W_n \quad (3)$$

$$LIR\ (\%) = W_L/W_m,\ SIR\ (\%) = W_S/W_m \quad (4)$$

W_t: the tumor weight of experimental group; W_n: the tumor weight of control group. W_L: liver weight of test group; W_S: spleen weight of test group; W_m: body weight of mice in each group.

2.9. H&E staining

In order to detect the toxicity of different administration methods to mice, all mice were killed 24 h after the last administration. The tumor, liver and spleen were taken from Saline, PTX Injection, PTX NPs + NIR and PTX NPs Gel + NIR group of autopsies, and each tissue section was stained with Hematoxylin-eosin (H&E) by light microscope (Nikon Eclipse E100, NikonDS-U3, Japan).

2.10. Statistical analysis

Statistical analysis was conducted via F test with IBM SPSS Statistics, version 19 (IBM Co., Armonk, NY). $^{*}P < 0.05$ or less statistically significant.

3. Results

3.1. Particle diameter and morphology

The average hydrated particle size of PTX NPs was (210.20 ± 1.57) nm (Fig. 1A), the PDI value was 0.081 ± 0.003, and the potential was (15.80 ± 0.35) mV. The average hydrated particle size of PPy NPs was (229.30 ± 1.35) nm (Fig. 1B), the PDI value was 0.165 ± 0.007, and the potential was (14.00 ± 0.05) mV.

Fig. 1C and D are electron microscope photographs of the prepared PTX and PPy NPs. From the figure, it can be seen that the PTX NPs have a regular rod-like structure and uniform distribution, while the PPy NPs can still be seen to have a spherical structure and good dispersion despite the size reduction caused by water loss during the sample preparation process. It is beneficial for nanoparticles to enter tumor cells and give better play to the curative effect (Sun et al., 2022).

3.2. Stability of medium

PTX NPs and PPy NPs did not appear turbidity or precipitation after 12 h incubation at 37 °C, and the particle size did not increase significantly, indicating that PTX NPs and PPy NPs could stably exist in saline, glucose and PBS (Fig. 2). The experimental results proved the stability of the two kinds of nanoparticles and also provide a research basis for the subsequent selection of drug delivery media.

3.3. Phase transition temperature

According to Table 2, the impact of varying concentrations of Poloxamer 188 on the gel phase transition temperature was observed when the concentration of Poloxamer 407 was fixed at 20.5% (mass fraction). The results indicated that when the concentration of Poloxamer 407 is fixed, the phase transition temperature will increase with the increase of Poloxamer 188 concentration. And the phase transition temperature changed after the addition of PTX NPs, which may be related to the mutual contact between nanoparticles and Poloxamer in the gel to promote their cross-linking. Specifically, when the concentration of Poloxamer 188 was 2% (mass fraction), the phase transition temperature was approximately 37 °C. This temperature aligns with the solution state required for *in vitro* injection under room temperature conditions. Subsequently, after injection, a phase transition occurs *in vivo*, resulting in the desired gel state for achieving a slow release of the drug. Considering the experimental results of phase transition and actual research needs, the concentration of Poloxamer 407 was chosen to be 20.5% (mass fraction) and the concentration of Poloxamer 188 was chosen to be 2% (mass fraction) to meet the needs of *in vitro* injection.

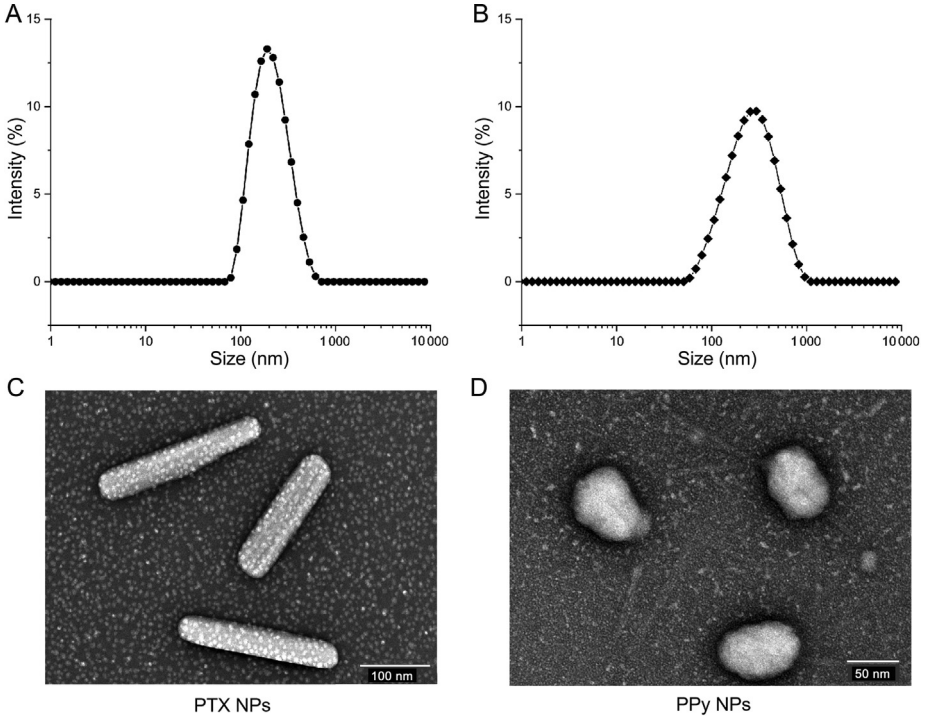

Fig. 1. Particle size distribution curve of (A) PTX NPs and (B) PPy NPs; TEM images of (C) PTX NPs and (D) PPy NPs.

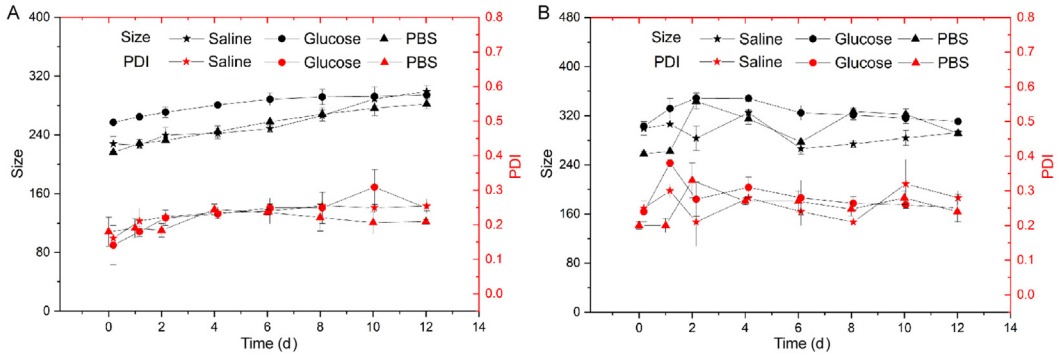

Fig. 2. The size and PDI diagrams for stability of PTX NPs (A) and PPy NPs (B) in physiological media (n = 3).

Table 2
Effects of different proportions of gel materials on gel phase transition temperature.

P407 + P188 (%)	Blank gel	PTX NPs gel
20.5 % + 1 %	32.9 °C	> 50.0 °C
20.5 % + 1.5 %	36.8 °C	31.6 °C
20.5 % + 2 %	37.2 °C	37.4 °C

3.4. Photothermal conversion performance

In order to eliminate the influence of thermometer material and other environmental factors, a comparative analysis using water as a control was conducted. Aqueous solutions with various concentrations of PPy NPs were irradiated for 350 s using a laser with a power density of 3.5 W/cm^2. Fig. 3 displays the results obtained to determine the optimal laser irradiation conditions for PPy NPs under 808 nm near-infrared. As can be seen in Fig. 3, the temperature increased significantly when different concentrations of PPy NPs solutions were irradiated with different power, while, water was little affected by it. In addition, the photothermal conversion performance increased with the increase of material concentration (Chu & Dupuy, 2014). After laser irradiation for 350 s, the temperature of PPy NPs could rise above 42 °C when the concentration was 0.5 mg/mL, which meets the requirements of clinical patients for treating diseases (Abdeltawab, Svirskis, & Sharma, 2020; Habibi, Sadat Shandiz, Salehzadeh, & Moradi-Shoeili, 2020; Kasinski, Zielinska-Pisklak, Oledzka, & Sobczak, 2020), and also reduces the dose of photothermal materials under the same circumstances, so the selection of 0.5 mg/mL of PPy NPs irradiated at 3.5 W/cm^2 laser for 350 s for subsequent experiments.

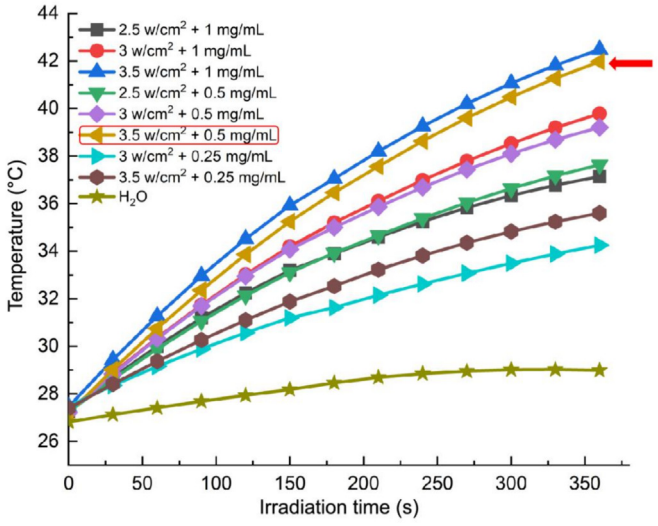

Fig. 3. Photothermal conversion performance of PPy NPs with different concentrations under different photothermal powers.

3.5. In vitro cell experiments

3.5.1. In vitro cytotoxicity assay

The experimental results were shown in Fig. 4A. Following a 48-h incubation of breast cancer cells with PPy NPs, the 4 T1 cells demonstrated robust cell activity, with a cell survival rate exceeding 86% at a high concentration of 20 mg/mL PPy NPs. This indicates excellent biocompatibility of PPy NPs, and the *in vivo* biosafety of PPy NPs has also been proved in previous animal studies (Sun et al., 2022). Moreover, when irradiated with a 3.5 W/cm^2 laser, the breast cancer cells exhibited more than 50% cell death at a concentration of 1.5 mg/mL PPy NPs (Fig. 4B), highlighting the exceptional photothermal properties of PPy NPs. It can also be seen from Fig. 4B that the cell survival rate further decreased as the concentration of PPy NPs continued to increase, and the experimental results showed that the IC_{50} value of PPy NPs on 4 T1 cells under 3.5 W/cm^2 laser irradiation was 1.107 mg/mL. The MTT results also showed that the IC_{50} value of PTX injection on 4 T1 cells was 1.737 μg/mL, while the IC_{50} value of PTX NPs on 4 T1 cells was 0.490 μg/mL (Fig. 4C and D). From the inhibition of 4 T1 cells *in vitro*, PTX NPs was more sensitive to 4 T1 breast cancer cells and had better anti-tumor effect than commercially available injections. The ability was about 3.5 times higher than that of commercially available PTX injection, which proved the antitumor superiority of PTX NPs administration.

3.5.2. In vitro cell uptake experiment

The results of cell uptake *in vitro* were shown in Fig. 4E, where green fluorescence represents the Coumarin-6 labeled drug, and blue fluorescence represents the nucleus labeled with DAPI. The green fluorescence intensity of PTX NPs Gel group is relatively weaker than that of PTX NPs group, indicating that PTX NPs Gel group has a certain sustained release effect on the drug. In addition, the drug labeling fluorescence intensity of PTX NPs + NIR group was significantly enhanced, indicating that near infrared could promote the uptake of PTX NPs by 4 T1 cells. However, in the PTX NPs Gel + NIR group, the fluorescence intensity of the drug labeling was weaker compared to the PTX NPs + NIR group. This could be attributed to the addition of photothermal materials and the gel phase transition induced by near-infrared stimulation. These factors might impede the release of the drug, thus affecting the rate at which the drug enters the cell. During the time of cell uptake investigation, the amount of gel-based drugs entering the cells was relatively small, and after the addition of NIR stimulation,

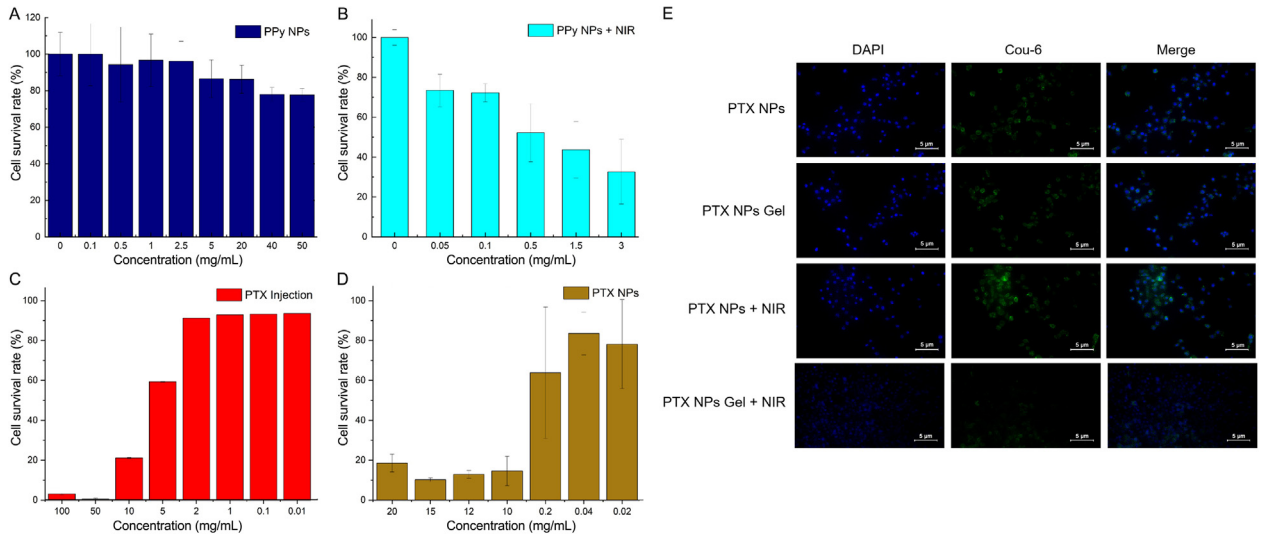

Fig. 4. (A) *In vitro* cytotoxicity studies of PPy NPs against 4 T1 cells at 72 h. (B) *In vitro* cytotoxicity studies of PPy NPs + NIR against 4 T1 cells at 72 h. (C) *In vitro* cytotoxicity studies of PTX Injection against 4 T1 cells at 72 h. (D) *In vitro* cytotoxicity studies of PTX NPs against 4 T1 cells at 72 h. (E) Fluorescence images of 4 T1 cells incubated with different drugs for 1 h (n = 6).

the drug uptake further decreased, which was related to the characteristics of temperature-sensitive gel. After NIR stimulation, the temperature increased and the phase transition accelerated, resulting in slow drug release, but the specific mechanism remains to be further studied (Ahmed et al., 2020; Chen et al., 2021).

3.6. In vivo experiment

3.6.1. Experiment on tissue distribution in mice

The results depicted in Fig. 5A demonstrate that within 24 h following intratumoral injection, the labeled drug's fluorescence appeared at the tumor site in each group, with no significant decrease in fluorescence intensity. This suggests that through intratumoral administration, the drug remains effective at the tumor site for an extended period of time. Furthermore, 24 h after administration, we observed that the fluorescence signal at the tumor site was stronger in the PTX NPs + NIR group compared to the PTX NPs group and PTX NPs Gel group. This indicates that NIR radiation can enhance the distribution of chemotherapeutic drugs within the tumor site.

Interestingly, the accumulation of PTX NPs Gel + NIR at the tumor site was significantly higher than that of PTX NPs + NIR. This observation may be attributed to the local temperature increase caused by near-infrared stimulation and the potential inhibition of PTX release in the gel form. However, further experiments are necessary to determine the precise mechanism behind this phenomenon. Compared with *in vivo* imaging, tissue distribution imaging *in vitro* can reduce the fluorescence noise of skin, avoid the interference of hemoglobin on blood flow in mice, and reduce the fluorescence attenuation in the process of tissue penetration, so that the fluorescence signals of different tissues and organs can be detected clearly. Therefore, the mice were euthanized 24 h later, and the tissues and organs were obtained after dissection, and the distribution of labeled PTX NPs in different organs was observed. As shown in Fig. 5B, the fluorescence of PTX injected via caudal vein is mainly distributed in the liver, followed by tumor and spleen. This may due to the formation of a large number of Dir nanoparticles during hemodilution after intravenous injection of PTX, which are only absorbed by Kupffer cells in the liver system. The fluorescence of each intratumoral injection group was mainly distributed in the tumor site, indicating that intratumoral injection had high drug aggregation, and the fluorescence intensity of PTX NPs Gel + NIR group was higher than that of PTX NPs + NIR group, which was consistent with the results of *in vivo* imaging, showing the superiority of combined administration.

3.6.2. In vivo pharmacodynamics experiment

The treatment plan was shown in the Fig. 6A. The frequency of administration in the intravenous injection group was once every two days, with a total of 7 times of administration. In view of the good efficacy of local administration and easy scabbing, the frequency of administration in the intratumoral injection group was set as 3 times of injection within 12 d (Zuo et al., 2022).

The tumor growth curves of mice in each group were shown in Fig. 6C, from which we can see that the tumor volume of normal saline negative control group was increased rapidly every day, while the tumor volume of positive control group slowed down. The therapeutic effects of PTX NPs and PTX NPs Gel were 48.64% and 56.79%, respectively. And the daily tumor volume changes were consistent. However, the anti-tumor effect of PTX NPs + NIR (91.05%) was much better than that of PTX NPs Gel + NIR (48.98%). This may be due to the cross-linking phenomenon between the drug and the gel directly loaded into the hydrogel system, and the drug diffused more slowly from the hydrogel matrix under the stimulation of NIR, so the anti-tumor effect of the gel was much lower than that of the NPs group. However, many influencing factors remain to be studied (Abdeltawab et al., 2020; Kasinski et al., 2020). From the experimental data of each group, photothermal combined with local chemotherapy has obvious advantages in the treatment of breast cancer, and the anti-tumor effect of PTX NPs group is more significant. Besides, the tumor inhibition rate of PTX NPs intratumoral injection of 2 mg/kg was similar to that of intravenous injection of PTX Injection 8 mg/kg. It shows that local administration has a certain advantage over intravenous administration. Local administration can make the drug act directly on the tumor site, reduce the process of systemic circulation in tail vein injection, and greatly increase the concentration of the drug in the tumor site, thus significantly improve the anti-tumor effect.

In the evaluation of drug toxicity, we typically assess mice based on their hair condition, feeding status, and changes in body weight. Throughout the feeding period, except for the mice in the

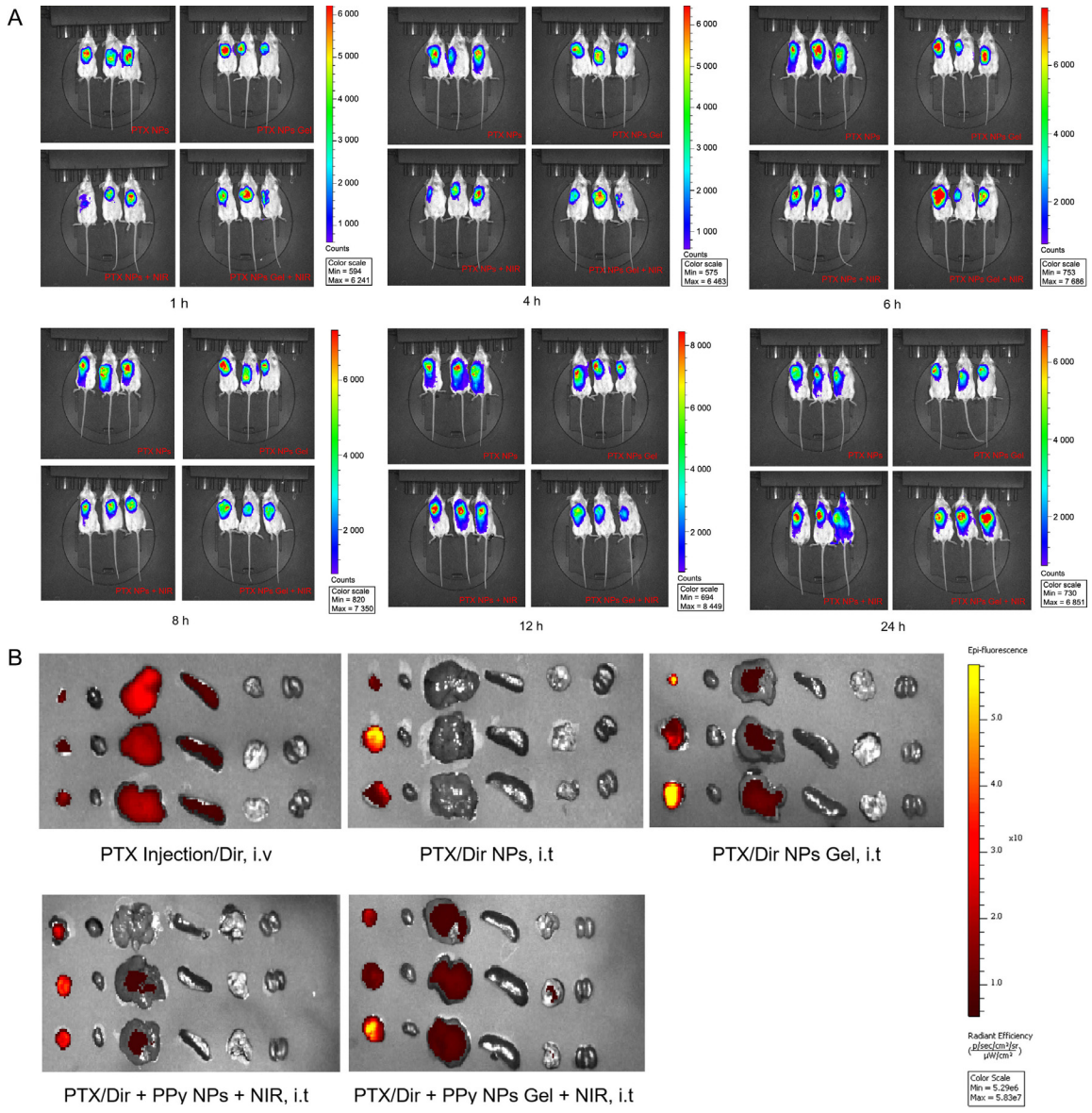

Fig. 5. Dynamic tissue distribution in 4 T1 tumor-bearing mice of each group (A); Tissue distribution of PTX NPs with different dosage forms in mice *in vitro* (tumor, heart, liver, spleen, lung, kidney from left to right) (n = 3) (B).

PTX injection group who displayed obvious fried hair and a curled-up appearance, the other groups exhibited normal hair and maintained a regular diet. Additionally, the body weight of the mice is presented in Fig. 6E. Notably, there were no significant differences in body weight among the experimental groups, indicating that all treatments were well-tolerated by the mice. Moreover, the photothermal treatment did not exhibit any significant toxic effects on the mice. After 12 d of administration, all mice were executed and their major organs were collected for further histological examination. The liver and spleen indices were calculated, and the results revealed no significant difference in the liver index between all administration groups and the normal saline group. However, the spleen index was notably lower in the PTX tail vein and intratumoral injection group compared to the normal saline group. There was no significant difference in spleen index between the combined administration gel group and normal saline group, suggesting that different administration modes of PTX could cause damage to the spleen of mice. However, the combined photothermal administration of PTX and PPy in the form of gel can reduce the damage to the spleen (Fig. 6F). The results of drug efficacy and tissue distribution *in vivo* showed that local administration of chemotherapeutic drugs combined with photothermal therapy can increase the drug concentration at the tumor site and reduce the drug distribution in normal tissues and organs, so as to enhance the anti-tumor effect and reduce systemic toxicity.

3.7. H&E staining

From the H&E staining shown in Fig. 7, there was no obvious damage to the organs in the normal saline group, and the tumor cells arranged irregularly and grew well. Compared with saline group, the PTX Injection group displayed more pronounced liver and spleen damage, along with increased infiltration of inflammatory cells and tumor cells (Chen et al., 2012). However, in PTX NPs Gel + NIR group, there was no obvious liver injury, spleen injury was alleviated, and tumor tissue injury was aggravated. In PTX NPs + NIR group, evident liver injury was absent, and spleen injury was mitigated, albeit with aggravated tumor tissue damage. Con-

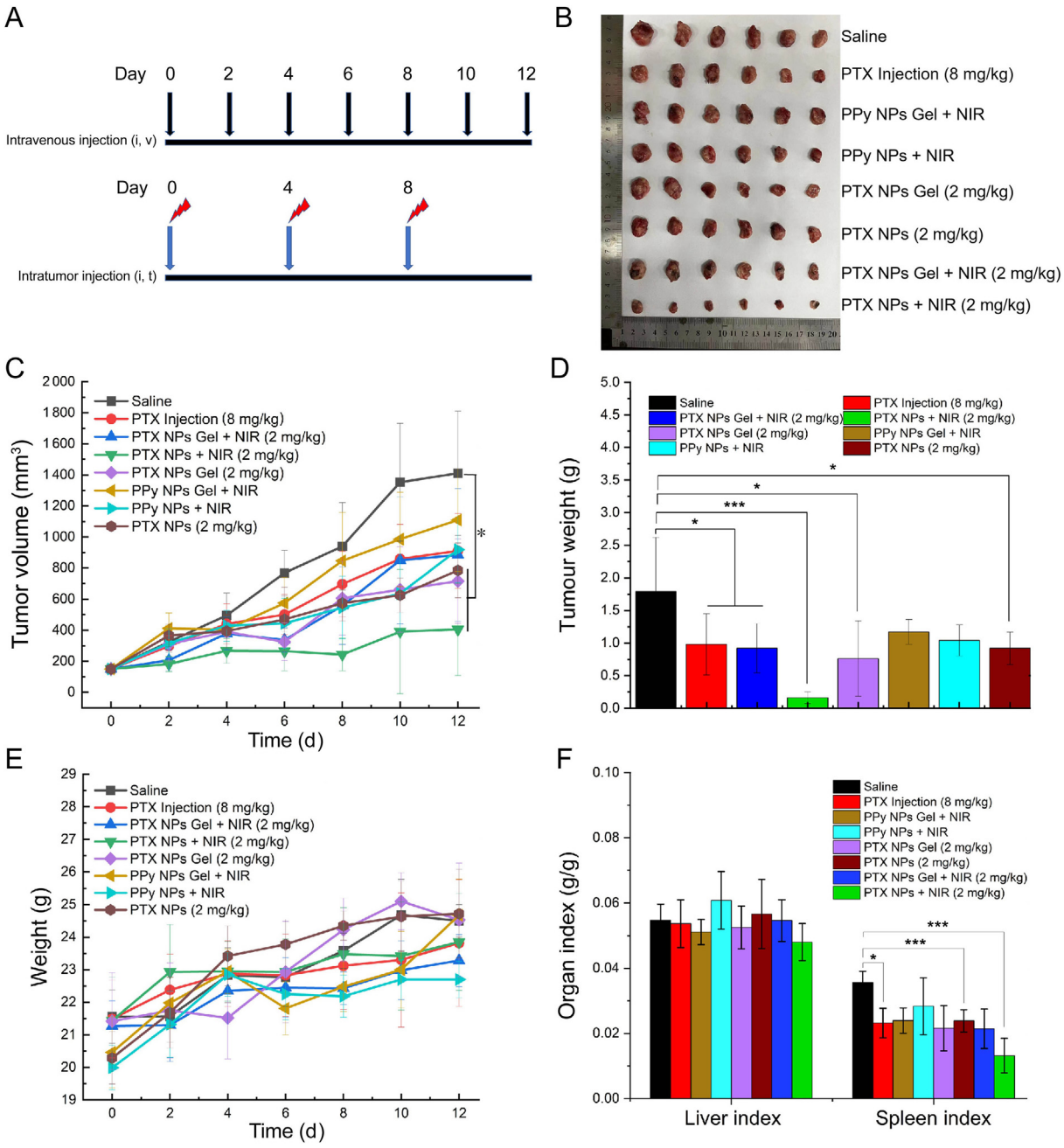

Fig. 6. Treatment schedule scheme: intravenous injection and intratumoral injection (A); Anatomical diagram of all groups of solid tumors at the end of the experiment (B); Schematic diagram of tumor growth curve of mice in each group during drug administration (C) (mean ± SD, $n = 6$); Tumor weight (D) (mean ± SD, $n = 6$); Body weight curve of each group during administration (E) (mean ± SD, $n = 6$); Organ index (F) (mean ± SD, $n = 6$). $^{*}P < 0.05$, $^{***}P < 0.001$.

versely, the PTX NPs + NIR group exhibited no noticeable liver and spleen injury. However, the tumor tissue showed the presence of multinucleated cells, tumor giant cells, some vacuolization, and cytoplasmic dissolution (Sun et al., 2022). These findings suggested that the combination of PTX with the photothermal material PPy NPs can reduce the liver and spleen injury induced by PTX while enhancing the anti-tumor effect.

4. Discussion

In this study, the current clinical antineoplastic drug PTX was selected as the chemotherapeutic drug to explore the efficacy of nanoparticles and gel in the treatment of breast cancer. First of all, we prepared PTX NPs and PTX NPs Gel, using PCL2k-mPEG2k as stabilizer, PTX NPs was prepared by anti-solvent precipitation method. Under transmission electron microscope, we can see that PTX NPs is a regular rod-like structure, and in the stability experiment, PTX NPs can exist stably in three physiological media, which can be used in subsequent experiments. PPy NPs was prepared by one-step polymerization, which showed a uniform spherical structure under the observation of transmission electron microscope, and could exist stably in three physiological media. Then, we investigated the photothermal conversion performance of PPy NPs. The experimental results show that when polypyrrole of 0.5 mg/mL is irradiated with near-infrared light with photothermal power of 3.5 w/cm^2, the temperature of PPy NPs can rise to more than 42 °C, which can effectively kill cancer cells, which proves

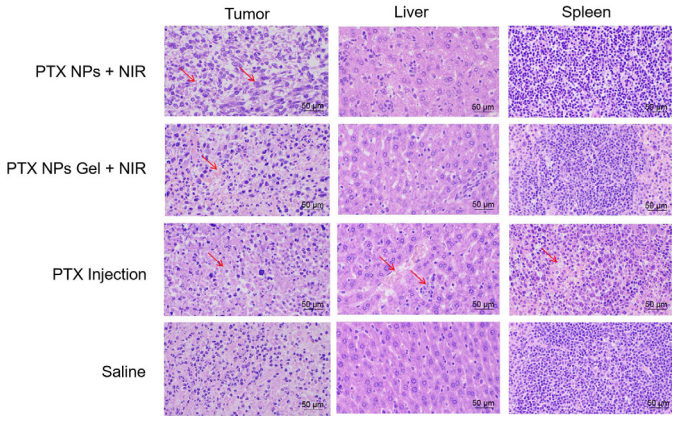

Fig. 7. H&E staining of tumor, liver and spleen (× 400). The place indicated by the red arrow is the site of injury or lesion.

that PPy NPs have excellent photothermal conversion properties. We selected P407 and P188 as the best concentration ratio of drug-loaded gel materials, which is beneficial for our administration and drugs to form gel in time and release drugs continuously in the form of semi-solid reservoir. Then, we studied the successfully prepared PTX NPs and PTX NPs Gel *in vivo* and *in vitro*. It was found that PPy NPs had good cell biocompatibility without NIR irradiation, while 1.5 mg/mL PPy NPs could kill more than half of the tumor cells when irradiated by NIR, which proved that PPy NPs could be used as a photothermal material for combined experiments *in vivo*. *In vitro* cytotoxicity test showed that the sensitivity of PTX NPs to breast cancer was higher than that of PTX. We studied the therapeutic effects of two different dosage forms of PTX NPs and found that drug-loaded gel could form a semi-solid reservoir at the injection site and maintain the blood concentration at the focus site, thus effectively treating breast cancer. Based on the analysis of the above experimental results, we concluded that the combined administration of nanoparticles can play the function of "1 + 1 > 2", but the existence of light and heat will affect the release of PPy NPs and PTX NPs from the drug-loaded gel, which may lead to the cross-linking phenomenon between the drug and the gel due to the direct loading of nano-drugs in the hydrogel system. Under the stimulation of NIR and release, the drug diffusion from the hydrogel matrix is slower, but many influencing factors remain to be studied.

5. Conclusion

The results showed that the intratumoral administration of PPy NPs and PTX NPs can significantly enhance the anti-tumor effect and reduce the toxicity. The efficacy and toxicity were studied in two dosage forms of nanoparticles and hydrogel, in order to compare the differences in dosage forms so as to achieve the purpose of treating breast cancer. On the basis of existing research, the synergistic of chemotherapy and photothermal provide a feasible and effective strategy for the treatment of tumors.

CRediT authorship contribution statement

Lina Sun: Data curation, Formal analysis, Visualization, Writing – original draft. **Cuiling Zuo:** Writing – review & editing. **Baonan Ma:** Data curation, Formal analysis. **Xinxin Liu:** Visualization. **Yifei Guo:** Conceptualization. **Xiangtao Wang:** Supervision, Writing – review & editing. **Meihua Han:** Conceptualization, Data curation, Project administration, Validation, Writing – original draft, Writing – review & editing.

Declaration of competing interest

The authors declare that they have no known competing financial interests or personal relationships that could have appeared to influence the work reported in this paper.

Acknowledgments

This work was financially supported by CAMS Innovation Fund for Medical Sciences (CIFMS, No. 2021-I2M-1-031, No. 2021-I2M-1-071). The Graphical Abstract was drawn using Figdraw.

References

Abdeltawab, H., Svirskis, D., & Sharma, M. (2020). Formulation strategies to modulate drug release from poloxamer based in situ gelling systems. *Expert Opinion on Drug Delivery, 17*(4), 495–509.
Ahmed, S., Alhareth, K., & Mignet, N. (2020). Advancement in nanogel formulations provides controlled drug release. *International Journal of Pharmaceutics, 584*, 119435.
Arnold, M., Morgan, E., Rumgay, H., Mafra, A., Singh, D., Laversanne, M., ... Soerjomataram, I. (2022). Current and future burden of breast cancer: Global statistics for 2020 and 2040. *Breast, 66*, 15–23.
Chen, J., Gu, H., Fu, S., Lu, J., Tan, H., Wei, Q., & Ai, H. a. (2021). Multifunctional injectable hydrogels for three-in-one cancer therapy: Preoperative remission via mild photothermal-enhanced supramolecular chemotherapy and prevention of postoperative recurrence and adhesion. *Chemical Engineering Journal, 425*.
Chen, M., Fang, X., Tang, S., & Zheng, N. (2012). Polypyrrole nanoparticles for high-performance *in vivo* near-infrared photothermal cancer therapy. *Chemical Communications, 48*(71), 8934–8936.
Chen, M. T., Sun, H. F., Zhao, Y., Fu, W. Y., Yang, L. P., Gao, S. P., ... Jin, W. (2017). Comparison of patterns and prognosis among distant metastatic breast cancer patients by age groups: A SEER population-based analysis. *Scientific Reports, 7*(1), 9254.
Choi, H., Kwon, M., Choi, H. E., Hahn, S. K., & Kim, K. S. (2021). Non-invasive topical drug-delivery system using hyaluronate nanogels crosslinked via click chemistry. *Materials (Basel), 14*(6).
Choudhury, H., Gorain, B., Tekade, R. K., Pandey, M., Karmakar, S., & Pal, T. K. (2017). Safety against nephrotoxicity in paclitaxel treatment: Oral nanocarrier as an effective tool in preclinical evaluation with marked *in vivo* antitumor activity. *Regulatory Toxicology and Pharmacology, 91*, 179–189.
Chu, K. F., & Dupuy, D. E. (2014). Thermal ablation of tumours: Biological mechanisms and advances in therapy. *Nature Reviews Cancer, 14*(3), 199–208.
Ding, F., Mou, Q., Ma, Y., Pan, G., Guo, Y., Tong, G., ... Zhang, C. (2018). A crosslinked nucleic acid nanogel for effective siRNA delivery and antitumor therapy. *Angewandte Chemie-international Edition, 57*(12), 3064–3068.
Fahad Ullah, M. (2019). Breast cancer: Current perspectives on the disease status. *Advances in Experimental Medicine and Biology, 1152*, 51–64.
Ghoncheh, M., Pournamdar, Z., & Salehiniya, H. (2016). Incidence and mortality and epidemiology of breast cancer in the world. *Asian Pacific Journal of Cancer Prevention, 17*(S3), 43–46.
Habibi, A., Sadat Shandiz, S. A., Salehzadeh, A., & Moradi-Shoeili, Z. (2020). Novel pyridinecarboxaldehyde thiosemicarbazone conjugated magnetite nanoparticulates (MNPs) promote apoptosis in human lung cancer A549 cells. *Journal of Biological Inorganic Chemistry, 25*(1), 13–22.
Han, M. H., Zheng, H., Guo, Y. F., Wang, Y. H., Qi, X. Y., & Wang, X. T. (2016). Novel folate-targeted paclitaxel nanoparticles for tumor targeting: Preparation, characterization, and efficacy. *Royal Society of Chemistry Advances, 6*(51), 45664–45672.
Huang, X., El-Sayed, I. H., Qian, W., & El-Sayed, M. A. (2006). Cancer cell imaging and photothermal therapy in the near-infrared region by using gold nanorods. *Journal of the American Chemical Society, 128*(6), 2115–2120.
Ibrahim, J. S., Hanafi, N., El-Tayeb, T. A., & Sliem, M. A. (2022). Polypyrrole-Gold nanocomposites as a promising photothermal agent: Preparation, characterization and cytotoxicity study. *Spectrochimica Acta Part A: Molecular and Biomolecular Spectroscopy, 264*, 120221.
Kasinski, A., Zielinska-Pisklak, M., Oledzka, E., & Sobczak, M. (2020). Smart hydrogels - synthetic stimuli-responsive antitumor drug release systems. *International Journal of Nanomedicine, 15*, 4541–4572.
Katsura, C., Ogunmwonyi, I., Kankam, H. K., & Saha, S. (2022). Breast cancer: Presentation, investigation and management. *British Journal of Hospital Medicine, 83*(2), 1–7.
Kievit, F. M., & Zhang, M. (2011). Surface engineering of iron oxide nanoparticles for targeted cancer therapy. *Accounts of Chemical Research, 44*(10), 853–862.
Kim, M. A., Shin, S. R., Kim, H. J., Lee, J. S., & Lee, C. M. (2022). Chemo-photothermal therapeutic effect of chitosan-gelatin hydrogels containing methotrexate and melanin on a collagen-induced arthritis mouse model. *International Journal of Biological Macromolecules, 218*, 1013–1020.
Kim, S. Y., & Lee, Y. M. (2001). Taxol-loaded block copolymer nanospheres composed of methoxy poly(ethylene glycol) and poly(ε-caprolactone) as novel anticancer drug carriers. *Biomaterials, 22*(13), 1697–1704.

Korzhikov-Vlakh, V., & Tennikova, T. (2021). Nanogels capable of triggered release. *Advances in Biochemical Engineering-Biotechnology, 178*, 99–146.

Lal, S., Clare, S. E., & Halas, N. J. (2008). Nanoshell-enabled photothermal cancer therapy: Impending clinical impact. *Accounts of Chemical Research, 41*(12), 1842–1851.

Li, W., Wang, X., Wang, J., Guo, Y., Lu, S. Y., Li, C. M., ... Liu, H. (2019). Enhanced photoacoustic and photothermal effect of functionalized polypyrrole nanoparticles for near-infrared theranostic treatment of tumor. *Biomacromolecules, 20*(1), 401–411.

Melero, I., Castanon, E., Alvarez, M., Champiat, S., & Marabelle, A. (2021). Intratumoural administration and tumour tissue targeting of cancer immunotherapies. *Nature Reviews Clinical Oncology, 18*(9), 558–576.

Nolsoe, C. P., Torp-Pedersen, S., Burcharth, F., Horn, T., Pedersen, S., Christensen, N. E., et al. (1993). Interstitial hyperthermia of colorectal liver metastases with a US-guided Nd-YAG laser with a diffuser tip: A pilot clinical study. *Radiology, 187*(2), 333–337.

Qi, W. X., Wang, S. L., Yang, H., Gao, K., Wang, Y. T., Sun, Y. D., ... Zhang, J. (2022). Preparation and *in vitro* evaluation of human serum albumin nano-drug delivery system loaded with paclitaxel for chemo-photodynamic combined therapy of breast cancer. *Chinese Traditional and Herbal Drugs, 53*(4), 993–1003.

Singla, A. K., Garg, A., & Aggarwal, D. (2002). Paclitaxel and its formulations. *International Journal of Pharmaceutics, 235*(1–2), 179–192.

Sun, L., Zuo, C., Liu, X., Guo, Y., Wang, X., Dong, Z., & Han, M. (2022). Combined photothermal therapy and *Lycium barbarum* polysaccharide for topical administration to improve the efficacy of doxorubicin in the treatment of breast cancer. *Pharmaceutics, 14*(12).

Theune, L. E., Buchmann, J., Wedepohl, S., Molina, M., Laufer, J., & Calderon, M. (2019). NIR- and thermo-responsive semi-interpenetrated polypyrrole nanogels for imaging guided combinational photothermal and chemotherapy. *Journal of Controlled Release, 311–312*, 147–161.

Tian, Y., Zhang, J., Tang, S., Zhou, L., & Yang, W. (2016). Polypyrrole composite nanoparticles with morphology-dependent photothermal effect and immunological responses. *Small, 12*(6), 721–726.

Vogel, A., & Venugopalan, V. (2003). Mechanisms of pulsed laser ablation of biological tissues. *Chemical Reviews, 103*(2), 577–644.

Weaver, B. A. (2014). How Taxol/paclitaxel kills cancer cells. *Molecular Biology of the Cell, 25*(18), 2677–2681.

Wu, Q., Li, J., Zhu, S., Wu, J., Chen, C., Liu, Q., ... Sun, S. (2017). Breast cancer subtypes predict the preferential site of distant metastases: A SEER based study. *Oncotarget, 8*(17), 27990–27996.

Yang, K., Xu, H., Cheng, L., Sun, C., Wang, J., & Liu, Z. (2012). *In vitro* and *in vivo* near-infrared photothermal therapy of cancer using polypyrrole organic nanoparticles. *Advanced Materials, 24*(41), 5586–5592.

Yu, D. L., Lou, Z. P., Ma, F. Y., & Najafi, M. (2022). The interactions of paclitaxel with tumour microenvironment. *International Immunopharmacology, 105*, 108555.

Zeng, N., Dumortier, G., Maury, M., Mignet, N., & Boudy, V. (2014). Influence of additives on a thermosensitive hydrogel for buccal delivery of salbutamol: Relation between micellization, gelation, mechanic and release properties. *International Journal of Pharmaceutics, 467*(1–2), 70–83.

Zha, Z., Yue, X., Ren, Q., & Dai, Z. (2013). Uniform polypyrrole nanoparticles with high photothermal conversion efficiency for photothermal ablation of cancer cells. *Advanced Materials, 25*(5), 777–782.

Zhu, L., & Chen, L. (2019). Progress in research on paclitaxel and tumor immunotherapy. *Cellular & Molecular Biology Letters, 24*, 40.

Zhu, S., Dou, M., & Huang, G. (2018). Intratumoral injection administration of Irinotecan-loaded microspheres: *In vitro* and *in vivo* evaluation. *AAPS PharmSciTech, 19*(8), 3829–3838.

Zuo, C., Zou, Y., Gao, G., Sun, L., Yu, B., Guo, Y., ... Han, M. (2022). Photothermal combined with intratumoral injection of annonaceous acetogenin nanoparticles for breast cancer therapy. *Colloids and Surfaces B: Biointerfaces, 213*, 112426.